Topological properties of bulk and edge states in honeycomb lattice photonic crystals: the case of TE polarization

2010 J. Phys.: Condens. Matter 22 225502

(http://iopscience.iop.org/0953-8984/22/22/225502)

IOP Publishing Journal of Physics: Condensed Matter

J. Phys.: Condens. Matter **22** (2010) 225502 (6pp) doi:10.1088/0953-8984/22/22/225502

Topological properties of bulk and edge states in honeycomb lattice photonic crystals: the case of TE polarization

Tetsuyuki Ochiai

Quantum Dot Research Centre, National Institute for Materials Science (NIMS), Tsukuba 305-0044, Japan

E-mail: OCHIAI.Tetsuyuki@nims.go.jp

Received 29 March 2010, in final form 26 April 2010
Published 21 May 2010
Online at stacks.iop.org/JPhysCM/22/225502

Abstract

Topological properties of bulk and edge states in honeycomb lattice photonic crystals are investigated theoretically for transverse-electric (TE) polarization. Breaking of space-inversion and time-reversal symmetries is considered at optical frequencies. The bulk band structure exhibits a topological phase transition by changing the degree of the broken symmetries. The resulting phase diagram correlates with zigzag and armchair edge states, and the so-called bulk–edge correspondence is verified. The effects of flat interfaces near the edges are also discussed.

1. Introduction

In the last few decades, artificial photonic materials have attracted much interest for realizing ultra-compact photonic integrated circuits [1] where active and passive photonic elements must be loaded in a controllable manner. Among them, non-reciprocal elements are important for flow control of light [2]. They can work in optical isolators and circulators. Traditional designs of a non-reciprocal element often employ the Faraday geometry and lack compactness. Recently, several researchers have demonstrated that non-reciprocal and one-way light waveguides can be realized, in a completely different design, by using certain magnetic photonic crystals (PhCs) under Voigt geometry [3–8]. Such waveguides can be compact and their usage in photonic integrated circuits is promising. We should also note that light transport in one-way waveguides is generally robust against disorder. The robustness is quite favourable for actual fabrication of waveguides, which inevitably includes disorder.

The robustness in the one-way transport is closely related to topological properties of eigenstates in the host medium around the waveguide. If the counter-propagating waveguide modes and bulk modes are absent in the frequency range concerned, the backscattering in the waveguide and the scattering into bulk are prohibited. Such a situation appears most typically in the sample edge of quantum Hall systems, where the drift motion of electrons along the sample edge forms chiral edge states of electrons. In this system, a topological relation between bulk and edge, which is called the bulk–edge correspondence, holds [9]. Roughly speaking, this theorem tells us that if bulk electronic states are topologically nontrivial, then edge electronic states can be chiral (one-way). The nontrivial topology of bulk electronic states is measured with the Chern number of Bloch band and results in nonzero quantized Hall conductance [10].

Recently, the author and his collaborator have argued the validity of the bulk–edge correspondence in photonic systems, within the context of the topological phase transition [11]. However, the system studied in the work is still restrictive and further investigation on the validity is necessary. In this paper, we investigate the bulk–edge correspondence and the topological phase transition in a different system of different polarization, where more nontrivial photonic band structure emerges in visible frequency ranges. Since the rigorous proof of the bulk–edge correspondence is still lacking in photonic systems, we need more evidences to establish this statement. Moreover, we need to know to what extent photonic systems are different from electronic ones from the viewpoint of topology. To do so, considering extreme cases that show clear contrast to electronic systems is effective. The aim of this paper is to demonstrate that the bulk–edge correspondence is certainly satisfied even if the vector-like nature of light and the flat interfaces near PhC edges are taken into account.

2. Bulk states

Suppose that a photonic crystal consists of a two-dimensional (2d) honeycomb array of two types of circular cylinders (called A and B) embedded in a magneto-optical substance. If A is different from B, then the space-inversion symmetry (SIS) is broken [12, 13]. Moreover, if a static magnetic field is applied parallel to the cylindrical axis, the time-reversal symmetry (TRS) is broken. These two broken symmetries can cause a topological phase transition. In the transverse-magnetic (TM) polarization, photonic systems are more or less similar to electronic systems which satisfy the scalar Schrödinger equation. In addition, in the gigahertz frequency range, a large magneto-optical effect is available. Thus, a simple analogy to quantum Hall systems can be drawn for the TM polarization [5]. In contrast, the vectorial nature stands out in the transverse-electric (TE) polarization, and the magneto-optical effect via a permittivity tensor is generally small in the visible frequency range. We thus have a completely different system, far from the quantum Hall system, in the TE polarization. Therefore, it is important to clarify how the topological phase transition and chiral edge states appear in the TE polarization.

To be specific, let us assume the dielectric constant of the cylinders ϵ_i ($i = \mathrm{A}, \mathrm{B}$) is high ($\sim$12). The radius of the cylinders is fixed as $r_i = 0.2a$, where a is the lattice constant. We further employ the free-electron metal model for the magneto-optical substance. Under a static magnetic field parallel to the cylindrical axis (the z axis), the permittivity tensor $\overleftrightarrow{\epsilon}$ of the free-electron metal at frequency ω becomes

$$\overleftrightarrow{\epsilon} = \begin{pmatrix} \epsilon_m & \mathrm{i}\alpha_m & 0 \\ -\mathrm{i}\alpha_m & \epsilon_m & 0 \\ 0 & 0 & \epsilon_{zm} \end{pmatrix}, \tag{1}$$

$$\epsilon_m = \epsilon_\infty \left(1 - \frac{\omega_\mathrm{p}^2(\omega + \frac{\mathrm{i}}{\tau})}{\omega\left(\left(\omega + \frac{\mathrm{i}}{\tau}\right)^2 - \omega_\mathrm{c}^2\right)} \right), \tag{2}$$

$$\alpha_m = -\epsilon_\infty \frac{\omega_\mathrm{p}^2 \omega_\mathrm{c}}{\omega\left(\left(\omega + \frac{\mathrm{i}}{\tau}\right)^2 - \omega_\mathrm{c}^2\right)}, \tag{3}$$

$$\epsilon_{zm} = \epsilon_\infty \left(1 - \frac{\omega_\mathrm{p}^2}{\omega\left(\omega + \frac{\mathrm{i}}{\tau}\right)} \right), \tag{4}$$

where ω_p and ω_c are plasma and cyclotron frequencies, respectively, τ is the relaxation time, and ϵ_∞ is the scalar permittivity at $\omega \to \infty$. The permeability tensor is taken to be unity throughout the PhC.

The photonic band structure of the TE polarization is shown in figure 1 for the PhC with both SIS and TRS. The band structure is calculated with the photonic Korringa–Kohn–Rostoker method [14, 15]. Here, we assume $\omega_\mathrm{p} a/(2\pi c) = 1$ and consider optical frequencies, because ω_p takes a value from visible to ultraviolet. The physical origin of the rather flat photonic bands in figure 1 is the coupling among the localized states of the isolated cylinders. In the frequency range of interest, the diagonal permittivity ϵ_m is negative, and the off-diagonal component α_m is set to be zero. Therefore, the free-electron metal screens the electro-magnetic field. As a consequence, bound modes localized in the isolated cylinder emerge with real eigenfrequencies. The eigenfrequencies of the localized states are determined by

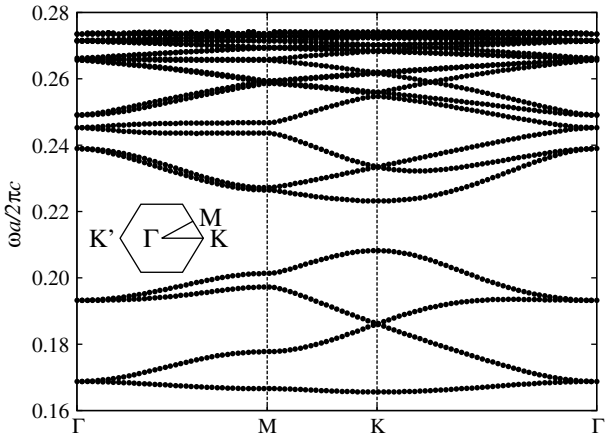

Figure 1. The photonic band structure of the TE polarization for the honeycomb lattice of dielectric cylinders embedded in a free-electron metal. The radius and the dielectric constant of the cylinders are taken to be $0.2a$ and 12, respectively, where a is the lattice constant. The following parameters are assumed for the free-electron metal: $\epsilon_\infty = 1$, $\omega_\mathrm{p} a/(2\pi c) = 1$, and $\omega_\mathrm{c} = \tau^{-1} = 0$.

$$\rho_m J_l'(\rho_i) H_l(\rho_m) = \rho_i \left(H_l'(\rho_m) + \frac{l\alpha_m}{\epsilon_m \rho_m} H_l(\rho_m) \right) J_l(\rho_i), \tag{5}$$

$$\rho_i = \frac{\omega}{c}\sqrt{\epsilon_i} r_i, \qquad \rho_m = \frac{\omega}{c}\sqrt{\frac{\epsilon_m^2 - \alpha_m^2}{\epsilon_m}} r_i. \tag{6}$$

A sequence of solutions is found at $\omega a/(2\pi c) = 0.1869$ ($l = \pm 1$), 0.2383 ($l = \pm 2$), 0.2577 ($l = \pm 3$), 0.2659 ($l = \pm 4$), 0.2670 ($l = \pm 5$), and so on, at $\omega_\mathrm{c} = \tau^{-1} = 0$, where l is the angular momentum. The mode of $l = 0$ is not found in the frequency range of interest. The interaction among nearby cylinders results in the frequency dispersion in the band diagram. Thus, this system has a close resemblance to the tight-binding model based on atomic orbitals.

Taking into account that there are two rods per unit cell, and that the bound modes are degenerate between l and $-l$, the lowest four bands are composed mainly of the multi-pole components of $l = \pm 1$. It is remarkable that these four bands are disconnected from other higher bands, but are connected within themselves at Γ, K, and K′. Moreover, we can see clearly a band touching with linear dispersion at K (and K′) between the second and the third bands. This so-called Dirac cone [16] can appear in triangular-like PhCs, and is a source of peculiar light-transport phenomena [17–20]. The degeneracy at Γ is lifted by the TRS breaking, whereas it is not lifted by the SIS breaking. On the other hand, the degeneracy at K is lifted both by the TRS breaking and by the SIS breaking. As a result, by applying a static magnetic field parallel to the cylindrical axis, which breaks the TRS, the four bands separate among other. Besides, by introducing a difference between A and B cylinders, which breaks the SIS, a gap opens in the Dirac cone, while the bands are still connected at Γ.

As for the TM polarization, the bottom of the photonic bands is at about $\omega a/2\pi c = 0.3$. Therefore, in the frequency range of interest no TM photonic band exists. As a consequence, the possible photonic band gaps between the lowest four TE bands are not affected by small perturbations which mix the TE and the TM polarizations. Such perturbations include the disorder that breaks the translational invariance in the z direction, the anisotropy in the permittivity and/or the permeability tensors that mix in-plane (x and y) and out-of-plane (z) components, and the bi-isotropy [21].

In what follows, we consider the parameter space spanned by two symmetry-breaking parameters. One is $\epsilon_A - \epsilon_B$, which describes the SIS breaking, and the other is ω_c, which describes the TRS breaking. The phase diagram regarding the Chern numbers of the four bands is shown in figure 2. Here, the Chern number of the nth band is defined by

$$C_n = \frac{1}{2\pi}\int_{BZ} d^2k(\nabla_{\boldsymbol{k}} \times \boldsymbol{\Lambda}_{n\boldsymbol{k}})_z, \tag{7}$$

$$\boldsymbol{\Lambda}_{n\boldsymbol{k}} = -i\langle n\boldsymbol{k}|\nabla_{\boldsymbol{k}}|n\boldsymbol{k}\rangle, \tag{8}$$

$$= \frac{-i}{A_{UC}}\int_{UC} d^2x\mu_0 u^*_{n\boldsymbol{k}}(\boldsymbol{x})\nabla_{\boldsymbol{k}}u_{n\boldsymbol{k}}(\boldsymbol{x}), \tag{9}$$

where $u_{n\boldsymbol{k}}(\boldsymbol{x})$ is the envelope function of the z-component of the magnetic field H_z for the nth Bloch mode at Bloch momentum $\boldsymbol{k}$, and is normalized as $\langle m\boldsymbol{k}|n\boldsymbol{k}\rangle = \delta_{m,n}$. The symbol $\nabla_{\boldsymbol{k}}$ stands for the gradient operator with respect to $\boldsymbol{k}$. There are six different phases each of which is bounded by the gap-closing curves. The gap-closing curve of Γ corresponds to $\omega_c = 0$, where the TRS is preserved. The Chern numbers of adjacent bands transfer on the curves as we change the parameters across the curves. This gives rise to the topological phase transition. This phase diagram is similar to that obtained before in [11, 22]. However, owing to the additional gap closing at Γ, the phase diagram becomes complicated.

The bulk–edge correspondence tells us that for a given gap, the sum of the Chern numbers of the Bloch bands below the gap is equal to the number of the chiral edge states in the gap. If the sum is negative, the chirality of the relevant edge states is inverted. According to this statement, in the upper right region with $(C_1, C_2, C_3, C_4) = (-1, 1, -1, 1)$, for instance, chiral edge states will appear in the gap between the first and the second bands (gap I) and the gap between the third and the fourth bands (gap III). The sum of the Chern numbers over the first and the second bands is zero, suggesting no chiral edge state appears in the gap between the second and the third bands (gap II). We can see this is just the case.

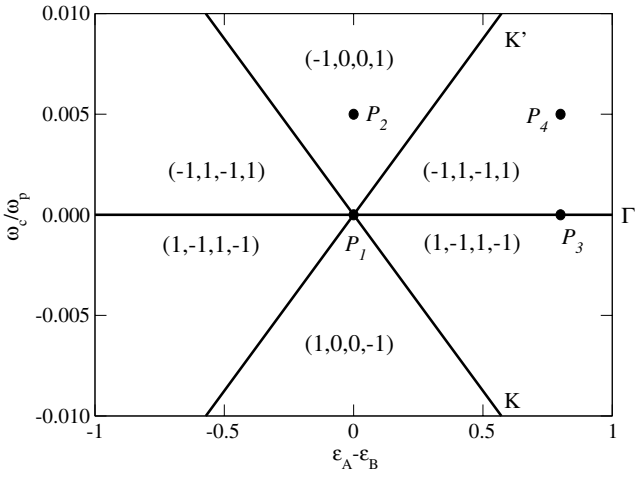

Figure 2. The phase diagram regarding the Chern numbers C_n of the lowest four bands. The Chern numbers are written in the format of (C_1, C_2, C_3, C_4). The diagram is spanned by two parameters, $\epsilon_A - \epsilon_B$ and ω_c, while the other parameters of the PhC as well as the average $(\epsilon_A + \epsilon_B)/2$ are kept fixed. The thick lines are the gap-closing curves of Γ, K, and K′.

3. Edge states

Next, we consider edge states (or in other words, surface states) for a stripe geometry with a finite number (N) of layers of the honeycomb lattice PhC with two parallel edges, upper and lower ones. To characterize the edge states, we assume zigzag and armchair edges with two kinds of geometry, either the presence or absence of an interface near the edge. In the PhC under consideration, the background medium is not empty. Therefore, the PhC edge is defined by fixing the distance d between the boundary column of the dielectric cylinders and the flat interface between the background medium and air. We consider two extreme cases, $d \to \infty$ and $d = d_{layer}/2$, where d_{layer} is the interlayer distance between two adjacent mono-layers. For the zigzag stripe, $d_{layer} = \sqrt{3}a/2$, whereas $d_{layer} = a/2$ for the armchair stripe. The stripe width is equal to Nd_{layer}. If $d \to \infty$, the edge states are screened irrespective of Bloch momentum. In contrast, if $d = d_{layer}/2$, the edge states are strongly influenced by the interface, and the light cone must be taken into account. Please refer to [11] for the calculation method employed in this paper.

3.1. Without an interface

Let us first consider the case of $d \to \infty$. Figure 3 shows the projected band diagram and the dispersion curves of the edge states relevant to the zigzag edge at four representative points in the phase diagram (figure 2).

In this projection the K and K′ points are mapped onto $k_\parallel a/2\pi = -1/3$ and $1/3$, respectively, where $k_\parallel$ stands for the Bloch momentum parallel to the edge. The band touching there for P_1 is due to the Dirac cone. For P_1 and P_3, the TRS is preserved, while the TRS is broken and nonzero Chern numbers are obtained for P_2 and P_4. We can see gap III is incomplete, whereas gap I and gap II can be complete (2d-omni-directional).

The dispersion curves of the edge states change their characteristics in accordance with the phase diagram. For P_1 all the curves are almost degenerate except around the Dirac point $k_\parallel a/2\pi = \pm 1/3$. The lifting of the degeneracy around the Dirac point is a finite-size effect, so that the complete degeneracy is obtained at $N \to \infty$ irrespective of $k_\parallel$. For P_3 it is still on the phase boundary and the degeneracy of the edge states in gap II is lifted. Notable features appear

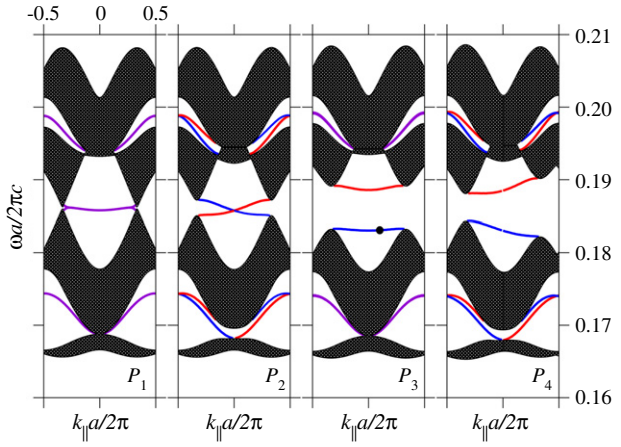

Figure 3. The projected band diagram and the dispersion curves of the edge states relevant to the zigzag edge at four representative points (P_n) in the phase diagram (figure 2). The shaded regions correspond to the bulk modes, otherwise the (pseudo) gap. The coloured curves represent the dispersion relation of the edge states. Red (blue) curves stand for localization in the upper (lower) edge of the PhC stripe. The violet curve represents localization in both the edges because of (approximate) degeneracy. The number of layers forming the zigzag PhC stripe is 16.

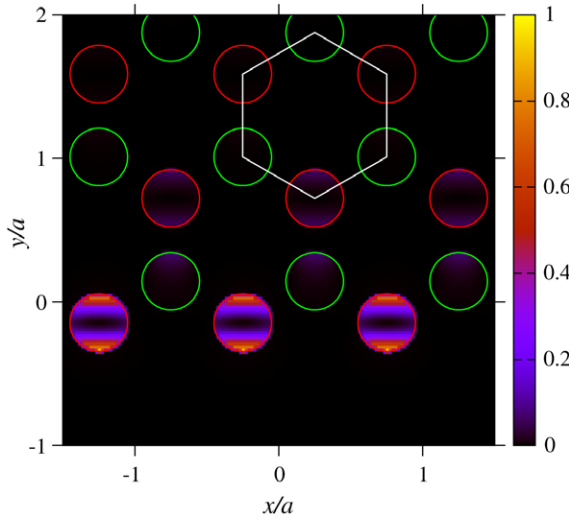

Figure 4. The magnetic field strength $|H_z|^2$ of the edge state at the marked point of P_3 in figure 3. The maximum field strength is normalized to be one. Red and green circles stand for the boundary of A and B cylinders, respectively, and the white line stands for the boundary of a unit cell.

for P_2 and P_4, where some of the bands have nonzero Chern numbers. For P_2 all the edge states are gap-less, that is, the dispersion curve traverses the gap between the nearby bands. Moreover, the edge states become chiral in the 2d-omni-directional gap region of gap I and gap II. Namely, the upper (lower) edge states, represented by red (blue) curves, have positive (negative) group velocities there and the counter-propagating mode with negative (positive) group velocity is absent within the upper (lower) edge. As a consequence, the dispersion curves of the upper and lower edge states cross each other at a particular point of $k_\parallel$. For P_4 the dispersion curves of the edge states in gap II do not cross each other, whereas the other curves in gap I and gap III cross. All of the above properties are consistent with the bulk–edge correspondence.

The rather flat dispersion curves in gap II of P_1 and P_3 are reminiscent of the flat-band edge states in zigzag graphene ribbons [23, 24]. To compare our system with graphene, let us consider the field configuration of the edge state. The magnetic field strength of the edge state at the marked point ($k_\parallel a/2\pi = 0.1$) of P_3 in figure 3 is shown in figure 4. Point P_3 lies on the phase boundary and can be obtained by a small perturbation from P_1, where the Dirac cone is obtained as in graphene. The field strength is strongly localized in the boundary row of the A cylinders, whereas non-negligible contributions are found in the nearby rows of the B and A cylinders. We should emphasize that the edge states under consideration exist only if $|k_\parallel|a/2\pi \leqslant 1/3$. In contrast, the flat-band edge states of graphene exist only if $|k_\parallel|a/2\pi \geqslant 1/3$. The edge states with $|k_\parallel|a/2\pi \leqslant 1/3$ are found also in the photonic analogue of graphene composed of metallic spherical particles [25]. Therefore, these features highlight a contrast between electronic and photonic systems. We also note that the field configuration inside the boundary A cylinders exhibits a p-wave-like behaviour, in agreement with the statement that the lowest four bulk bands are mainly composed of the p-wave ($l = \pm 1$).

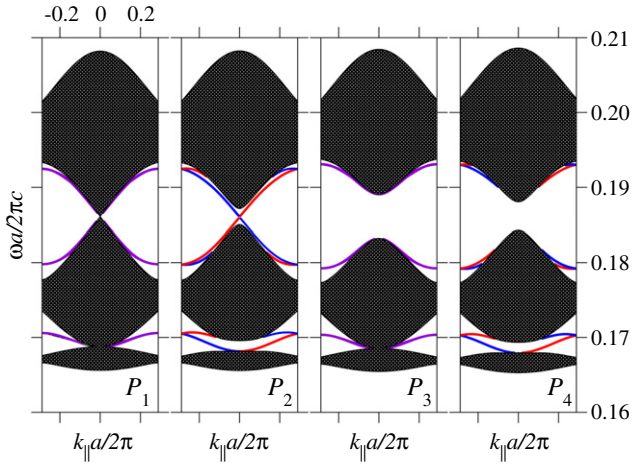

Figure 5. The projected band diagram and the dispersion curves of the edge states relevant to the armchair edge at four representative points in the phase diagram (figure 2). The number of layers forming the armchair PhC stripe is 16.

Figure 5 shows the projected band diagram and the edge states' dispersion curves relevant to the armchair edge. In this projection Γ, K, and K′ points are mapped onto the same point of $k_\parallel a/2\pi = 0$, and gap III is not visible. Thus, the bulk–edge correspondence is hidden there. The edge states in gap I and gap II exhibit a similar tendency as in the zigzag PhC stripe. That is, only if the relevant Chern numbers are nonzero as in P_2 and P_4, the dispersion curve of the edge states traverses the gap and the two curves (red and blue) cross each other at $k_\parallel a/2\pi = 0$ or ± 0.5. Moreover, the edge states become chiral in the 2d omni-directional gap.

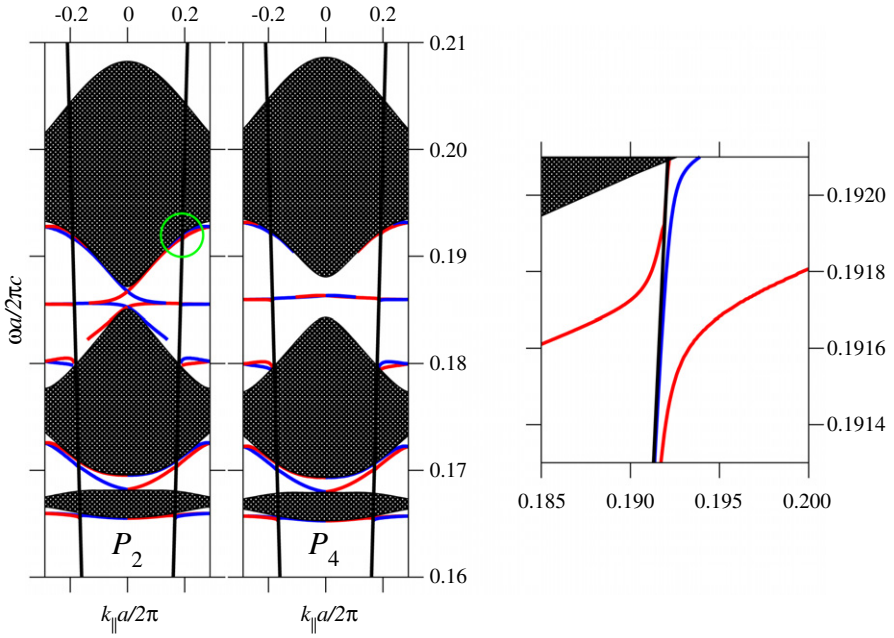

Figure 6. The projected band diagram and the dispersion curves of the edge states relevant to the armchair edges with flat interfaces at $d = d_{\text{layer}}/2$. Thick black lines stand for the light line. The number of layers is taken to be 64. The right panel is an enlarged figure around the green circle in the left panel.

3.2. With an interface

Next, we consider the effects of flat interfaces near the PhC edges. In the metallic background the flat interface alone supports the surface plasmon polariton (SPP) mode whose dispersion relation is given by the following equation,

$$\kappa_0 + \frac{\epsilon_m \kappa_m + \alpha_m k_\parallel}{\epsilon_m^2 - \alpha_m^2} = 0, \tag{10}$$

$$\kappa_0 = \sqrt{k_\parallel^2 - \frac{\omega^2}{c^2}}, \qquad \kappa_m = \sqrt{k_\parallel^2 - \frac{\epsilon_m^2 - \alpha_m^2}{\epsilon_m}\frac{\omega^2}{c^2}}. \tag{11}$$

In the frequency range of interest, the dispersion curve of the SPP is close to the light line $\omega = c|k_\parallel|$. The SPP mode does not have a nonzero cutoff frequency. In the stripe geometry with two flat interfaces, two SPP modes emerge. Besides, rather flat photonic band modes exist in bulk as shown in figure 1. The bulk and the two SPP modes mix strongly near the light line, forming 'meta-polaritonic' bands. In addition, the interfaces induce the coupling with the external radiation modes. As a consequence, the edge states are categorized into leaky and guided states, depending on whether they are inside or outside the light cone. The dispersion curve of the leaky edge states has a finite line width determined by the imaginary parts of the eigenfrequencies. Therefore, we must take account of this allowance in the bulk–edge correspondence. The leakage is inherent in photonic systems, because the air outside the photonic systems is not 'insulating'.

Figure 6 shows the projected band diagram and the dispersion curve of the edge states relevant to the armchair edges with the flat interfaces. The number of layers in the PhC stripe is increased to $N = 64$. The presence of the interface changes the dispersion curve from that in figure 5. For instance, we can find additional curves in gap II around $\omega a/2\pi c = 0.18$ and in the region just below the first band. However, we can still find a common feature in the dispersion curves. A remarkable difference of the dispersion curves between P_2 and P_4 is found in gap II. For P_2, the dispersion curve of the edge states does traverse the gap. However, that for P_4 does not. Therefore, chiral edge states are realized in gap II solely for P_2. As for gap I, chiral edge states emerge for both P_2 and P_4. All of these properties are consistent with the bulk–edge correspondence. It should be noted that the gap traverse is not obvious at small N ($\sim$16), because the line width of the relevant edge states is not small enough.

If we closely look at the dispersion curves near the light cone, anti-crossing of the curves takes place. This is due to the mixing of the SPP modes and edge modes of PhC origin. The mixing results in 'meta-polaritons'. In the right panel of figure 6, the upper 'meta-polariton' (red curve) is almost a pure edge state at $k_\parallel a/2\pi = 0.185$, but becomes SPP-like near the light line. Eventually, it merges with the bulk band. The middle and lower 'meta-polaritons' (blue and red curves, respectively) become SPP-like near the light line. These two lines are hidden in the left panel and are almost degenerate with the light line. Since there are always two light lines $\omega = ck_\parallel$ and $-ck_\parallel$, propagating and counter-propagating modes coexist at a given frequency. Thus, we may neglect their effect in the bulk–edge correspondence. Nevertheless, we should remember their presence, because they can readily mix with the edge modes of PhC origin.

4. Conclusion

In summary, we have investigated topological properties of bulk and edge states in honeycomb lattice PhCs for the TE

polarization. The breaking of the TRS and the SIS results in a rich phase diagram concerning the Chern numbers of Bloch bands in bulk. The Chern numbers are well correlated with the chirality of the edge states, and the bulk-edge correspondence has been verified in the PhC stripes with and without the flat interfaces. If the interfaces are absent, a similar but different edge state to that in graphene ribbon emerges. If the interfaces are present, the dispersion curves of the edge states have certain line widths if they are inside the light cone. In addition, the SPPs localized around the interfaces mix with the PhC edge states, forming 'meta-polaritons' in the vicinity of the light cone. These two features in the system with the interfaces show a strong contrast between electronic and photonic systems, and suggest novel functions inherent in light transport near the edge.

Acknowledgments

The author would like to thank M Onoda for valuable discussions. This work was partially supported by Grant-in-Aid under Grant No. 20560042 for Scientific Research from the Ministry of Education, Culture, Sports, Science, and Technology.

References

[1] Joannopoulos J D, Meade R D and Winn J N 1995 *Photonic Crystals* (Princeton, NJ: Princeton University Press)
[2] Nishihara H, Haruna M and Suhara T 1989 *Optical Integrated Circuits* (New York: McGraw-Hill)
[3] Haldane F D M and Raghu S 2008 *Phys. Rev. Lett.* **100** 013904
[4] Yu Z, Veronis G, Wang Z and Fan S 2008 *Phys. Rev. Lett.* **100** 023902
[5] Wang Z, Chong Y D, Joannopoulos J D and Soljačić M 2008 *Phys. Rev. Lett.* **100** 013905
[6] Takeda H and John S 2008 *Phys. Rev.* A **78** 023804
[7] Ao X, Lin Z and Chan C T 2009 *Phys. Rev.* B **80** 033105
[8] Wang Z, Chong Y D, Joannopoulos J D and Soljačić M 2009 *Nature* **461** 772–5
[9] Hatsugai Y 1993 *Phys. Rev. Lett.* **71** 3697–700
[10] Thouless D J, Kohmoto M, Nightingale M P and den Nijs M 1982 *Phys. Rev. Lett.* **49** 405–8
[11] Ochiai T and Onoda M 2009 *Phys. Rev.* B **80** 155103
[12] Cassagne D, Jouanin C and Bertho D 1996 *Phys. Rev.* B **53** 7134–42
[13] Onoda M and Ochiai T 2009 *Phys. Rev. Lett.* **103** 033903
[14] Leung K M and Qiu Y 1993 *Phys. Rev.* B **48** 7767–71
[15] Ohtaka K, Ueta T and Amemiya K 1998 *Phys. Rev.* B **57** 2550–68
[16] Geim A K and Novoselov K S 2007 *Nat. Mater.* **6** 183–91
[17] Sepkhanov R A, Bazaliy Y B and Beenakker C W J 2007 *Phys. Rev.* A **75** 063813
[18] Zhang X 2008 *Phys. Rev. Lett.* **100** 113903
[19] Sepkhanov R A, Ossipov A and Beenakker C W J 2009 *Europhys. Lett.* **85** 14005
[20] Zandbergen S R and de Dood M J A 2010 *Phys. Rev. Lett.* **104** 43903
[21] Lindell I V, Sihvola A H and Tretyakov S 1994 *Electromagnetic Waves in Chiral and Bi-Isotropic Media* (Norwood: Artech House Publishers)
[22] Raghu S and Haldane F D M 2008 *Phys. Rev.* A **78** 033834
[23] Fujita M, Wakabayashi K, Nakada K and Kusakabe K 1996 *J. Phys. Soc. Japan* **65** 1920–3
[24] Nakada K, Fujita M, Dresselhaus G and Dresselhaus M S 1996 *Phys. Rev.* B **54** 17954
[25] Han D, Lai Y, Zi J, Zhang Z Q and Chan C T 2009 *Phys. Rev. Lett.* **102** 123904